AUT Journal of Modeling and Simulation

AUT J. Model. Simul., 53(2) (2021) 137-152
DOI: 10.22060/miscj.2022.19713.5242

Heat Distribution in High Power Yb Doped Fiber Laser by Considering Photo-darkening Effect

Maryam Karimi*

Photonic and Quantum Technology Research School, Nuclear Science and Technology Research Institute, Tehran, Iran

ABSTRACT: Several effects, such as optical nonlinear and thermal effects can change and reduce the output power of high-power Fiber Laser. In this paper, the photodarkening effect, as an additional loss factor in the high-power Fiber Laser s, was added in the rate equations, and the pump power variation relation was rewritten under the new conditions. By considering the complete form of the heat transfer function, including conductive and radiative heat transfer, the generated heat in the double clad Fiber Laser with the bidirectional pump scheme for different cavity geometry was determined. In this paper, the photodarkening loss is added to the rate equations as power decreasing factor, which is suggested as a stretched exponential function. The effects of core radius, the first clad size, input power, output reflectors coefficient, and laser cavity length in the heat generation were calculated. The contribution of each heat production factor including Quantum Defect, photodarkening, and propagation loss were also determined in heat generation. It was shown that the share of photodarkening heat caused from pump power and propagation loss affected from pump power in heat generation in the Double clad Fiber Laser is negligible. However, the photodarkening heat affected from signal power is the main factor in heat generation at the central points of Fiber Laser.

Review History:

Received: Mar. 06.2021
Revised: Jan. 04, 2022
Accepted: Feb. 13, 2022
Available Online: Mar. 10, 2022

Keywords:

Double Clad Fiber Laser
Thermal Effects
Ytterbium Doped Fiber
Heat Distribution
Photodarkening
Effect, and Rate Equation.

1- Introduction

Use of Yb in the glass host for designing a laser has been considered since 1962 [1]. Yb3+ doped fiber glass with Ge co-dopant has broadband absorption and emission spectrum from 0.97-1.2 μm, hence, different kinds of power source can be used in wide choice of wavelength [2, 3].

Kilowatt Fiber Laser (FL) achieved by Yb3+-doped fiber, which operating near 1μm [4]. By increasing the effective area of the core, the output power of Fiber Lasers and amplifiers will be increased. Although in the large Mode Field Diameter (MFD) the nonlinear effects to be reduced [5, 6], in most cases, the large mode area active fibers are used for fabrication of high-power Fiber Lasers and amplifiers [7, 8], which the high-power causes to appear nonlinear effects in the environment. Photonic crystal fibers are suitable options for designing the large mode area single mode Fiber Lasers [9, 10]. The optical nonlinear effects such as Stimulated Raman Scattering (SRS), Stimulated Brillouin Scattering (SBS), and self or cross, phase modulation (SPM or XPM) can be used to make several types of equipments such as Raman or Brillouin Fiber Lasers and amplifiers, wavelength laser tuning, nonlinear spectroscopy, frequency metrology, ultra-fast laser and emerging technologies that make the quantum mechanical effects [11]. Mode Instability (MI) as thermal nonlinear phenomena is a disturbing effect that has not been introduced an application for it until recently [12]. MI is suppressed with different methods to increase the out power and beam quality [3, 13], tailoring the Yb-ion distribution, shifting of the pump or signal power, using the large first clad doped fiber, using different pump configuration [15], or coiling of the FL to decrease the higher order mode [14, 15, 16]. Several factors create heat in the fiber. The most reason for the heat creation in the high-power FL is the Quantum Defect (QD) [18, 17].

Quantum Defect heat arises from the energy difference between pump and signal photons [4]. Photo-darkening (PD) loss is another heat source which depends on the pump and signal wavelengths, seed power, and the fiber core size [4, 18, 19]. PD effect, which is also called photochromic damage or Photo-Induced Absorption, occurs when they are irradiated with light at certain wavelengths [20]. PD in Yb-doped Fiber Lasers is observed as a degradation in output laser power over time, limiting the operational lifetime. The material aspects of PD have been given considerable attention during the last two decades [21]. The PD takes place when the YDF is pumped at the Yb absorption band (916 nm/ 976 nm) or irradiated under visible wavelength of 488 nm [22]. PD increases the background loss from Ultraviolet to near infrared band and causes the absorption of pump light [23]. Additionally, PD-induced thermal load can cause a series of issues. It could change the refractive index of the optical fiber by the thermo-optic effect, and affecting

*Corresponding author's email: mykarimi@aeoi.org.ir

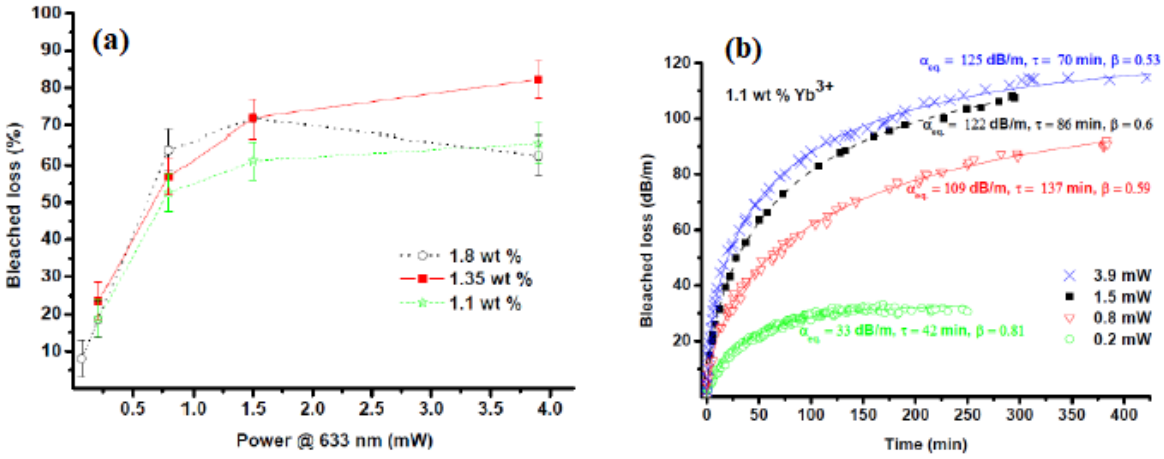

Fig. 1. a) Percentage of the photodarkening bleached loss as the function of laser power, b) Bleaching of 1.1 wt%, Yb3+ doped fiber for different at 633 nm [38].

the waveguide structure and thereby altering the bending loss of different modes [24]. More seriously, the thermal load induced by PD could distort the phase of the beam and aggravate thermally induced refractive index grating, which could eventually trigger the occurrence of Mode Instability (MI) [24]. The mechanism of PD has not been determined yet; however, researchers have made great efforts to suppress PD [24]. The PD problem is typically overcome by using Large-Mode-Area (LMA) fibers; but even with these fibers, Photo-Induced Absorption (PIA) has been observed [25]. The absorption occurs in the visible and near infrared originating from the creation of color centers in the silica network [25]. Different mechanisms have been proposed to explain the formation of color centers. This could be due to charge transfer, non-bridging Oxygen Holes, Oxygen Deficiency Centers (ODC), Yb2+ ions, or even Yb2+-Yb3+ pairs [26]. Some dopant such as aluminum with high concentration or Aluminum-phosphor can Suppress PD effect [24, 27-28]. Optimizing the doping composition by co-doping with Ce, P, Al, and Na ions into the fiber could inhibit PD to a certain extent [24]. Recently, a new method is proposed to reduce the PD in Fiber Laser and amplifiers [24, 29-30]. In this way, O_2 or H_2 loaded fiber exhibits excellent thermal performance in Fiber Lasers [24]. Propagation loss in the pump and signal wavelengths also increase the temperature at the Fiber Lasers and amplifiers [18, 31]. The physical description of the PD effect is interpreted with the creation or existence of the color centers [32, 33, 34]. The color centers have the absorption bands spread from Ultraviolet (UV) to visible, and have tails the near-infra-red [32, 35], where the pump and signal wavelengths are acted in the FL. In many doped fibers with the rare earth, such as Tm3+, Ce3+, Pr3+, Er3+, Tb3+, Yb3+, the PD effect has been reported [33, 34]. Different factors effect on the PD phenomena, claustration of Yb ions increases the PD effect [32]. Although the Yb/Al co-doped fiber have large absorption and emission cross-section and properly thermal property, the level of PD is high [36]. Some co-dopant such as cerium (Ce) or Phosphorus (P) in Yb/Al co-doped fiber can be useful to decrease the PD effects [36, 37]. In both cases, the emission and absorption cross-section of the doped fiber will be reduced the Yb concentration must be increased and to achieve the high gain, which causes the PD-loss, so the co-dopant concentration must be carefully selected to have lower MI in high power FL [37].

In the previous works, different definitions of the heat source at Fiber Lasers were classified and their simulation results were compared with each other [17]. In this work, the PD loss is added to the rate equations as a power decreasing factor. Under these changes, the effect of cavity parameters, such as core and first clad sizes, laser length, and the reflectors at the end of FL are investigated in the same bidirectional pump scheme in heat distribution.

2- Rating the Equations by Considering the Photo-darkening Loss in Fiber Lasers

The PD effect reduces the power of the signal (lasing) and pumps [34, 18]. Therefore, in the high-power Fiber Laser and amplifiers which the PD effect was sighted, the additional loss coefficient as PD loss can be inserted as power consumer at the rate equation. In the low pump power, the PD loss is negligible or near zero, but at the high-power FLs, this excess loss will be important. Therefore, we expect that the PD loss coefficient depends on the beam power; hence, the coefficient value rapidly increases in the certain power value. Since the number of color centers in the sample should be limited, after the special power value, the PD loss coefficient must be reached to a constant limit.

In Ref. [38], the experimental results of the Photo-Bleaching (PB) loss variation with respect to the incidence power at the 633 nm for different dopant concentration was represented, which is reshown in Fig. (1). As shown in Fig. (1-a), by increasing the pump power, PD loss increased in the sample, and in a 4 mW pump power, the loss approached the constant value. In Fig. (1-b), the variation of the bleached loss with respect to time is depicted. As seen in Fig. (1), the

trend of PD loss with respect to time and power are the same. In Ref. [24]; PD-induced excess loss with and without H_2-loaded in the fiber is depicted. The PD loss occurs in low level pump power between 16-86 mW. in Yb doped fiber [22]. As shown in Fig. (1), the experimental results show the PD loss variation with respect to the input power have stretched exponential function.

In Ref. [24, 53], a classical stretched exponential function used to fit the time variation of the PD effect. By comparing the two diagrams of Fig. (1 a,b), it is observed that they have the same trend. Therefore, in this paper the stretched exponential function in the form of $\alpha_{PD-\lambda}(I_\lambda) = A\left(1-\exp\left(-\varepsilon I_\lambda\right)\right)$ for the PD loss with respect to the input power is suggested; where, $\alpha_{PD-\lambda}$ is PD attenuation at selected wavelength λ, I_λ is the input pump power, and the e , A are constants with the positive values. The results of the PB loss were fitted on the stretched exponential function. If the PD loss has a similar trend to the PB loss, the suggested function for the excess loss can be matched on the experimental reality. Nonetheless, the value of the $a_{PD\text{-}l}$ can be considered as a constant value in the small increments of power. In this paper, it is assumed that the value of PD loss is constant at the considered pump value. The numerical solving of rate equations is the common method to investigate FL power variations [39], the rate equations are present by [17]:

$$\pm\frac{dP_\ell^\pm(z)}{dz} = \Gamma_\ell\left[\left(\sigma_\ell^e+\sigma_\ell^a\right)N_2(z)-\sigma_\ell^a N\right]\times P_\ell^\pm(z)-\alpha_\ell P_\ell^\pm(z) \quad (1)$$

$$\pm\frac{dP_p^\pm(z)}{dz} = -\Gamma_p\left[\sigma_p^a N-\left(\sigma_p^e+\sigma_p^a\right)N_2(z)\right]\times P_p^\pm(z)-\alpha_p P_p^\pm(z) \quad (2)$$

$$\frac{N_2(z)}{N} = \frac{\frac{\left[P_p^+(z)+P_p^-(z)\right]\sigma_p^a\Gamma_p}{h\upsilon_p A_{co}}+\frac{\left[P_\ell^+(z)+P_\ell^-(z)\right]\sigma_\ell^a\Gamma_\ell}{h\upsilon_\ell A_{co}}}{\frac{\left[P_p^+(z)+P_p^-(z)\right]\left(\sigma_p^a+\sigma_p^e\right)\Gamma_p}{h\upsilon_p A_{co}}+\frac{1}{\tau}+\frac{\left[P_\ell^+(z)+P_\ell^-(z)\right]\left(\sigma_\ell^a+\sigma_\ell^e\right)\Gamma_\ell}{h\upsilon_\ell A_{co}}} \quad (3)$$

Up to now, the effect of PD were created in rate equations with a α_{PD} as a constant PD loss coefficient [18]. The equation is always used when the pump power is high enough to start the PD effect. Therefore, to use the inclusion of the PD loss in the rate equation in any power, we must use the relation that changes the PD with power. The stretched exponential function can achieve the desired results in the Rate equations. In Relations (2 and 3), $P_p^\pm$, and $P_\ell^\pm$ are the + (forward) and - (backward) of the pump and lasing power, respectively. υ_p , and υ_ℓ are the frequency of the pump and lasing,. σ_ℓ^e , σ_ℓ^a, and σ_p^a are the emission and absorption cross-section of lasing, and absorption cross-section of the pump power, respectively. h is the Planck's constant, and τ is the steady-state lifetime. N is the dopant concentration in ion/m^3, and z is position along the fiber length. Γ_p , Γ_ℓ are the overlap factor at the pump and lasing wavelength, respectively. The overlap factor of the pump power in double-clad FL is estimated as $\Gamma_p \approx A_{co}/A_{cl1}$ [40, 41]. The overlap factor at the lasing wavelength is $\Gamma_\ell = 1-\exp\left(-2r_{co}^2/\omega^2\right)$, where r_{co} is the radius of the Fiber Laser core, and w is the spot size. For the Gaussian pulse shape, with number V in the range of 0.8-2.8, the experimental relation approximate of the spot size in the doped fiber can be used as follows [17]:

$$\omega = \rho\left(0.616+\frac{1.66}{V^{1.5}}+\frac{0.987}{V^6}\right) \quad (4)$$

α_p and α_ℓ are the background loss at the pump and laser wavelength, respectively. α_{PD-p} and $\alpha_{PD-\ell}$ are photodarkening loss at the pump and laser wavelength [18, 42] ,which is not considered at the rate equations for conventional FL. The photodarkening loss coefficient depends on the dopant concentration and determines from [18]:

$$\begin{aligned}
&\alpha_{PD^{633nm}}(dB/m) \approx 175\left(\frac{N}{8.74\times10^{25}}\right)^{2.09}\cdot\frac{N_2/N}{0.46};\\
&\alpha_{PD^{1\mu m}}(dB/m) \approx 175\left(\frac{N}{AFF\times8.74\times10^{25}}\right)^{2.09}\cdot\frac{N_2/N}{0.46}\cdot\frac{AFF}{\gamma};\\
&\gamma = 24.5; \quad PD^{633} = \frac{PD^{1\mu m}}{\gamma}\left(\frac{dB}{m}\right);
\end{aligned} \quad (5)$$

AFF is the area filling factor. Since the experimental results of PD loss is present in visible region [32, 35, 42] and the details of this loss in the pump and signal wavelength are not available, it is assumed in this paper that $\alpha_{PD-\ell} \approx \alpha_{PD-p} \approx \alpha_{PD^{1\mu m}}$, because there are not enough experimental results to replace the real values.

The pump variations can be determined independent of the signal (lasing) beam specifications [2].

$$\frac{dP_p(z)}{dz} = -\frac{Ah\nu_p}{\phi_p\tau}N_2(z) \quad (6)$$

In Eq. (6), ϕ_p is the pump quantum efficiency, which for Yb3+, $\phi_p \sim 1$ [2].

By combining Eq. (1) and (6) and the integration of the equation, the pump power variations along the fiber length obtain as follows:

$$\ln\frac{P_p^{\pm}(z)}{P_p^{\pm}(0)}+\frac{\phi_p\tau}{Ah\nu_p}\left[\left(\sigma_p^e+\sigma_p^a\right)-\frac{\ln 10}{10}\frac{C}{N}\right]\times \left(P_p^{\pm}(z)-P_p^{\pm}(0)\right)+\left(\sigma_p^a N\Gamma_p+\alpha_p\right)z=0 \quad (7)$$

$$C=175\cdot\left(\frac{N}{AFF\times 8.74\times 10^{25}}\right)^{2.09}\cdot\frac{AFF}{0.46\gamma}$$

3- Complete Heat Distribution Equation in Active Fibers

The heat distribution equation in the core and clads region of the Double-clad FL can be described by the thermal conduction equation in the cylindrical coordinate [43, 44].

$$\frac{1}{r}\frac{\partial}{\partial r}\left(r\frac{\partial T_{core}(r,z)}{\partial r}\right)=-\frac{Q(z)}{K_1},\quad (0\le r\le a) \quad (8)$$

$$\frac{1}{r}\frac{\partial}{\partial r}\left(r\frac{\partial T_{clads}(r,z)}{\partial r}\right)=0,\qquad (a\le r\le c) \quad (9)$$

where Q(r, z) , is the heat density per unit of volume (W/m^3). It is assumed in this paper that the generated heat from QD, PD, and background loss is as follows [18]:

$$Q_{12}(z)=Q_{QD}(z)+Q_{PD}^{P}(z)+Q_{PD}^{\ell}(z)+Q_{PL}^{p}(z)+Q_{PL}^{\ell}(z) \quad (10)$$

$$Q_{PL-i}(z)=\frac{\alpha_i}{A_m^i}\left(P_i^{+}(z)+P_i^{-}(z)\right);\ i=(s,p) \quad (11)$$

A_m^i : mode *area of the light* (*Pump or signal*)

α_i : Pr*opagation of loss due to absorption and not scattering*

$$Q_{PD}^{i}(z)=\frac{\Gamma_i Ln(10)PD^{1\mu m}}{10A_{co}}\left(P_i^{+}(z)+P_i^{-}(z)\right); \quad (12)$$

$$Q_{QD}(z)=(1-S)\frac{\Gamma_p\left(\sigma_p^a N_1(z)-\sigma_p^e N_2(z)\right)\left(P_p^{+}(z)+P_p^{-}(z)\right)}{A_{co}}; \quad (13)$$

$S=\lambda_p/\lambda_\ell$

In the above equations, T_{core} and T_{clad} are the temperature variation at the core and clad, respectively. Q_{QD}, Q_{PD}^{P}, Q_{PD}^{ℓ}, Q_{PL}^{p}, and Q_{PL}^{ℓ} are the heat produced from Quantum Defects (QD), photodarkening in pump power, photodarkening in laser (signal) power, propagation loss in pump wavelength, and propagation loss in laser (signal) wavelength. S is the quantum or optical conversion efficiency, which is λ_p/λ_ℓ. There is no heat source for the cladding regions a £ r £ c, and in Q(z) = 0, r, is the radial coordinate, z, is the longitudinal coordinate along the fiber, and K_1, is the thermal conductivity of silica. The thermal conductivity can have different coefficients for the core, and first and second clad of fiber. Heat is only created in the doped core region of the FL. T_{core} , and T_{clads} are the temperature at the core and cladding regions, respectively. The temperature and its derivatives must be continuous across the inner boundaries. Moreover, at the outer cladding-air interface, heat is transferred by convective and radiative heat flux [45, 46]. Thus, the following conditions are confirmed at the boundaries [17]:

$$dT_{core}(r=0,z)/dr=0\ \rightarrow T_{core}(r=0,z)=cte, \quad (14)$$

$$T_{core}(a,z)=T_{clad\,1}(a,z),\quad K_1\frac{dT_{core}(r=a,z)}{dr}=K_2\frac{dT_{clad\,1}(r=a,z)}{dr}, \quad (15)$$

$$T_{clad\,1}(b,z)=T_{clad\,2}(b,z),\quad K_2\frac{dT_{clad\,1}(r=b,z)}{dr}=K_3\frac{dT_{clad\,2}(r=b,z)}{dr}, \quad (16)$$

$$\frac{dT_{clad\,2}(r=c,z)}{dr}=\frac{h}{K_h}\left(T_c(r,z)-T_{clad\,2}(r=c,z)\right)+\frac{\sigma_b\varepsilon}{K_h}\left(T^4{}_c(r,z)-T^4{}_{clad\,2}(r=c,z)\right), \quad (17)$$

where h, is the heat transfer coefficient. The value of h depends on the environment temperature [47]. By assuming a constant value for the environment temperature in this paper, a constant value is considered for heat transfer coefficient. The values of K_1, K_2, and K_3, are the conductive heat transfer coefficients at the core, and first and second clads, respectively. K_h is the conductive heat transfer coefficients of the air. T_{core}, $T_{clad\,1}$, and $T_{clad\,2}$ are the temperature variation in the core, and first and second clads, respectively. T_c, is the environment temperature or the temperature that FL sustained. s_b is the Stefan-Boltzmann constant, e is the surface emissivity. Both Equations (10), and (11) consist of two boundary conditions (the temperature and its derivative are continuous at the boundaries); hence, there are six boundary conditions that determine all the constant values. By solving Eqs. (23), and (24) using boundary condition, the value of $T_{clad\,2}$ at the radial point r = c obtained as follows [17]:

$$f\left(T_{clad\,2}\left(r=c,z\right)\right)=\frac{\sigma_b\varepsilon}{K_h}T_{clad\,2}^4\left(r=c,z\right)+\frac{h}{K_h}T_{clad\,2}\left(r=c,z\right)-\frac{\sigma_b\varepsilon}{K_h}T_c^4-\frac{h}{K_h}T_c+\frac{Q\left(z\right)a^2}{2K_3c}=0 \quad (18)$$

Thus, the temperature changes in the core and clads as follows [17]:

$$T_{core}\left(r,z\right)=T_0\left(z\right)-\frac{Q\left(z\right)r^2}{4K_1}\qquad \left(0\le r\le a\right), \quad (19)$$

$$T_{clad\,1}\left(r,z\right)=-\frac{Q\left(z\right)a^2}{K_2}\ln r+Q\left(z\right)a^2\ln b\left(\frac{1}{k_2}-\frac{1}{k_3}\right)+T_{clad\,2}\left(r=c,z\right)+\frac{Q\left(z\right)a^2}{K_3}\ln c\qquad \left(a\le r\le b\right), \quad (20)$$

$$T_{clad\,2}\left(r,z\right)=-\frac{Q\left(z\right)a^2}{K_3}\ln r+\frac{Q\left(z\right)a^2}{K_3}\ln c+T_{clad\,2}\left(r=c,z\right)\qquad \left(b\le r\le c\right), \quad (21)$$

In the previous work, the heat distribution of double-clad Fiber Laser with the bidirectional pump scheme was simulated by considering different definitions of the heat source at FL, and the share of each factor in heat generation at double-clad FL with the relatively large first clad size was determined [17].

4- Simulation Results and Discussions

Using Eq. (6), the refractive index of the glass with 6% mole of GeO2 (x =6%) is determined as 1.4583 for the signal wavelength of 1090 nm. For fibers with the a 10 μm core size, the value of the V number is 2.3248. On the other hand, the laser operates single mode around 1090 nm. The overlap factor at the laser wavelength is about 0.813 from Eq. (7). The pump power must be calculated from Eq. (6) in order to calculate the signal (laser) output from the rate equation. Eq. (6) was numerically solved using the bisectional method [49]. By determining the pump power value at all fiber length, only Eq. (1) should be solved as a Boundary Value Problem (BVP) with the boundary conditions of $P_\ell^+=R_1P_\ell^-$ and $P_\ell^-=R_2P_\ell^+$ in the iterative algorithm. The fast and stable algorithm was used to get the numerical answers [50].

In this paper, only the bidirectional pump configuration is considered. The pump and lasing wavelengths are $\lambda_p=925\,nm$ and $\lambda_\ell=1090\,nm$, respectively. The Fiber Laser length is L = 20 m, and the grating reflection coefficients at the ends of the fiber R1 and R2 are 0.99 and 0.05, respectively. It is assumed in the present paper that there is no Bragg reflector at the pump wavelength; on the other hand, R3=0, [51, 52]. The other parameter values such as cross-sections, first and second clad radiuses, steady-state lifetime, background losses, input pump power and etc., are given in table (1).

The variations of the upper state level with respect to the position along FL for different first clad radiuses are depicted in Fig. (2a). As shown in Fig. (2a), for the smaller first clad radius, the upper state level density at the middle points of the fiber has the lower values. The reason is the pump power consumption at the initial regions of the FL elevates the electrons at the higher state level in the both ends of FL.

In comparison to the upper state density for the different first clad radius, the density has a larger value for the smaller first clad at the input region of FL, as shown in Fig. (2a). However, in the middle points from 3-17 m of FL, the upper state density decreases rapidly. By reducing the first clad radius from 200 to 100 μm, the density of the second level increases more than the twofold in the inputs of FL. For all of the first clad sizes, the density of higher state level has larger values at the input of FL. In Fig. (2b), the variation of the generated heat in FL with respect to the FL position for the different first clad radius is depicted. For small size of the first clad, the overlap factor of pump power with the doped region is higher, hence more power absorbed in the core and the laser power increases in the output. In this condition, the heat generation increases in FL. For all sizes of the first clad, the generated heat is higher at the end of FL; this issue is more obvious in the smaller first clad sizes in Fig. (2b). The reason is the presence of the reflector with a higher reflection coefficient at the input of FL and returning the laser power into the output end of FL. Therefore, the laser (signal) power is greater at the output respect to the input of FL (see Fig. (5a)). Thus, we expect the temperature to be higher at the output end of FL. By increasing the first clad size, the value of the generated heat significantly degrades in FL. According to Ref. [15-34], the MI decreases at the FL with large first clad, because of decreasing the pump absorption and consequently the temperature degrade at large first clad size. In Fig. (2c), the contribution of each factor in heat production for different first clad size is depicted. As shown in Fig. (2c), the Q_{QD} have the lower values at the middle points of FL for smaller first clad size. According to Eq. (12), the QD heat depends on the pump overlap factor. The value of G_p has a larger amount for the smaller size of the first clad, so the greater value of the pump power absorbed in the input points of FL and the level of the pump power decreases in the middle points in smaller size of first clad. Therefore, the values of QD heat have a larger value in the input ends of FL and lower amount at the middle points. The values of $Q_{PD-\ell}$ for different value of the first clad size are almost equal. According to Eq. (11), the

Table 1. Parameter values used in the of Heat distribution simulation at Yb DDCFL.

Parameters	Values (unit)
Emissivity	ε =0.85
Stefan-Boltzmann constant	σ_b=5.67×10^{-8} W/(m²·K^4)
Ambient temperature	T_c = 290 K
Core conductive heat transfer coefficient	K_1 =1.38
First clad conductive heat transfer coefficient	K_2 =1.38
Second clad conductive heat transfer coefficient	K_3 =0.2
Air conductive heat transfer coefficients	K_h =0.025 $Wm^{-1}K^{-1}$
Convective heat transfer coefficient	h=100 $Wm^{-2}K^{-1}$
laser wavelength (λ_ι)	λ_s=1090 nm
laser absorption cross-section [17]	σ_s^a=1.23×10^{-28} m^2
laser emission cross-section [17]	σ_s^e=1.24×10^{-25} m^2
Signal background loss	α_S=5 dB/km
Pump wavelength	λ_p= 925 nm
Pump absorption cross-section [17]	σ_p^a=6.64×10^{-25} m^2
Pump emission cross-section [17]	σ_p^e=4×10^{-26} m^2
Input pump power, FWP, BDP	P_p=500, 250 mW
Input pump power, BWP, BDP	P_p=500, 250 mW
Pump background loss [17]	α_P=3 dB/km
power filling factor	0.0025
Steady-state lifetime	T=0.84 s
dopant concentration	N_t=4×10^{25} ion/m^3
Active fiber length	L=20 m
Front Bragg reflector	R_1=0.98 at 1090 nm
back Bragg reflector	R_2=0.4 at 1090 nm

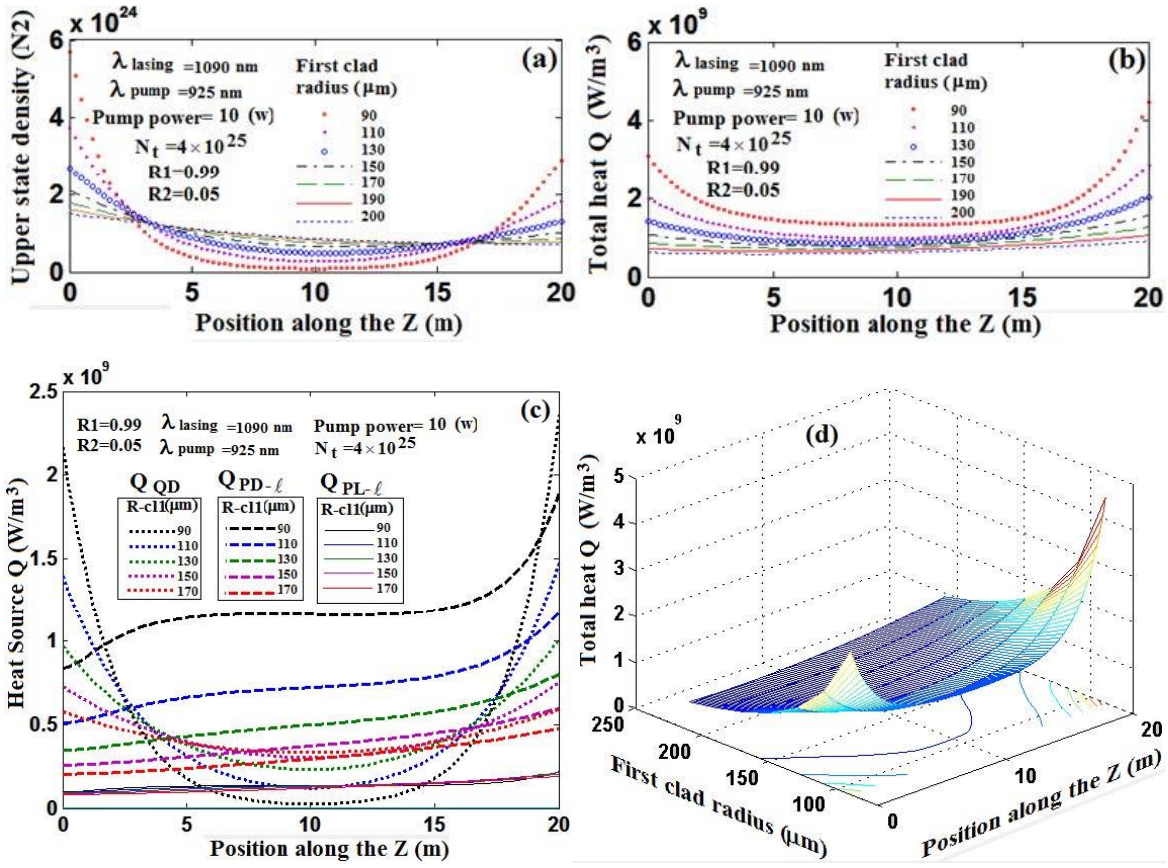

Fig. 2. variation of a) Upper state population, b) Total generated heat, c) share of QD, PD-ℓ, and PL-ℓ in heat generation with respect to fiber position for different first clad radius, d) 3D variation of total heat generation with respect to fiber position and first clad size.

PD heat in the signal or pump wavelengths depends on the overlap factor in each wavelength. In double clad Fiber Laser, the overlap factor fraction at the signal to pump power is about $100\left(\Gamma_s/\Gamma_p=\left(r_{clad1}/r_{co}\right)^2\simeq 100\right)$. So $Q_{PD-\ell}\simeq 100\,Q_{PD-p}$ and PD-P heat can be ignored in the calculation. As shown in Fig. (4a), the value of $Q_{PD-\ell}$ is larger because the pump absorption and consequently the signal power is larger at that first clad size for the smaller first clad radius.

The $Q_{PD-\ell}$ have larger values at the output end of FL since it has the maximum value of signal (laser) power. For each size of the first clad, the QD has more share in heat generation at the input and output end of FL than other factors. In the middle points of the FL, the PD is the main reason for increases in the FL temperature. Fig. (2d) shows the three-diminution variation of the total heat with respect to the FL position and first clad size. It should be noted that the variation of the Q_{PL-P} and Q_{PD-P} for heat generation is low and negligible, which was shown in Ref. [17] that the percentage of Q_{PL-P} and Q_{PD-P} for respectively large first clad can be ignored.

The research results show that the total heat and sequentially temperature decrease along with the Fiber Laser. The results of Ref [55, 17] show that the central axes of Fiber Laser have the maximum temperature that is compatible with the results of the present paper.

Effects of core size on heat generation in FL is investigated in Fig. (3). The dopant density is assumed to be constant in each core size. On the other hand, the number of dopants in the bigger core size is larger. Thus, to have a constant value for density in the calculations, the value of N is multiplied by r_{co}^2/r_{clad1}^2. As shown in Fig. (3a), by increasing the core size, the value of PD generated heat $Q_{PL-\ell}$ increased. In other words, the PD heat is the main reason for increasing FL temperature in the larger core size. According to Eq. (12), the QD heat is inversely proportional to the core area. In comparison to two FL with different core sizes and equal pump power, the pump power was rapidly absorbed in the input ends of FL with the larger core area. Hence, it is expected that the middle

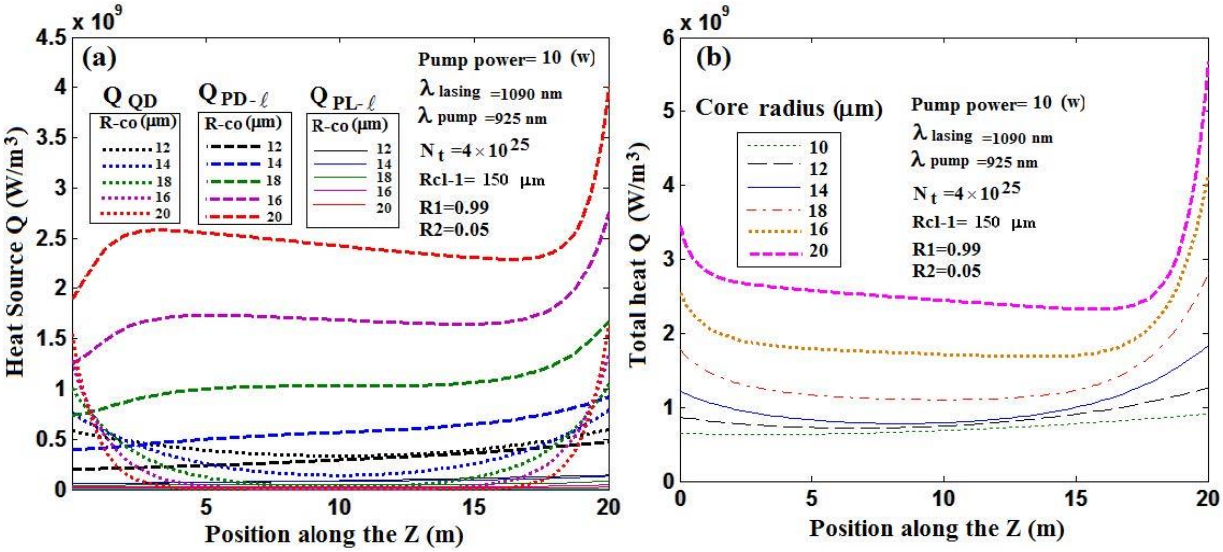

Fig. 3. Heat variation along the fiber position (a) Share of QD, PD-ℓ, and PL-ℓ in heat generation for different core size, b) Total heat variation vs. FL position for the different core size.

points of FL in the FL with the larger core have lower pump level and consequently lower heat generation from QD effect, which is confirmed in Fig. (3a).

According to Eq. (10), the PL heat generation is inversely proportional to mode area and depends directly on the signal (laser) power. In FL, the signal (laser) output is directly related to the pump power value. Thus, the laser output cannot grow from a certain level in FLs with the equal pump power. The mode area increases by increasing the core radius. As shown in Fig. (3a), by increasing the core size the value of PL, the generated heat is reduced but the magnitude of this change is negligible. Fig. (3b) shows the evolution of total heat generation Vs. core size. By increasing the core radius, the more heat is generated at the ends of FL; hence, the probability of FL damage is higher at the output of the FL due to the higher temperature in the FL with the larger core size.

Fig. (4); shows the three-dimensional variation of the total heat contribution in FL with respect to the FL position and the core radius. As shown in Fig. (4a), the generated heat at the input and output of the FL is greater and in the central points of FL is lower in the FL with the larger core size. The reason is the equal input pump power at the FLs with the different core size the pump power absorbed completely in the input points of FL with the larger core and the central points of FL do not sense the pump power. It should be noted that by increasing the core size, the optical nonlinear effect is reduced; however, the thermal nonlinear effect is added in the FL with larger core radius.

Fig. (4b) shows the PD generated heat with respect to the FL position and the FL core size. As observed, by increasing the core size, the $Q_{PD-\ell}$ increases at all areas of FL. However, this increment is slightly a higher value at the end put of FL. According to the existence of the reflector with the higher reflection coefficient at the input end of FL, the signal (lasing) at the output of FL have higher power and cause increasing of the heat generation at that point. As shown in Fig. (4c), by increasing the core size, the $Q_{PL-\ell}$ decreases due to Eq. (10) because the $Q_{PL-\ell}$ has an inverse relationship with the doped area. As seen in Fig. (4d), by duplicating of core radius from 10 to 20 mm, the generated heat increases up to threefold; on the other hand, the heat generation has a nonlinear relationship with the core size.

In Fig. (5a), the variation of P_ℓ^+ and P_ℓ^- with respect to the FL position for the different value of the reflection coefficient of the input reflector (R1) is shown. By increasing the R1 coefficient value, P_ℓ^+ increases and P_ℓ^- decreases. As shown in Fig. (5a), the variation of P_ℓ^- is relatively low. In Fig. (5b), the value of $\alpha_{PD-\ell}$ is calculated from Eq. (5), and is depicted with respect to the FL position for the different R1 values. As shown in this figure, by increasing the input mirror reflector coefficient, the value of $\alpha_{PD-\ell}$ decreases since by increasing the input reflector coefficient the signal power increases and the upper state level population decreases; therefore, according to Eq. (5), the value of $\alpha_{PD-\ell}$ decreases as well.

So far, variation of the reflection coefficient endpoint mirrors of the doped Fiber Laser in the thermal distribution of these devices has not been investigated. In Ref [54], the effect of the reflection coefficient of the mirrors in solid-

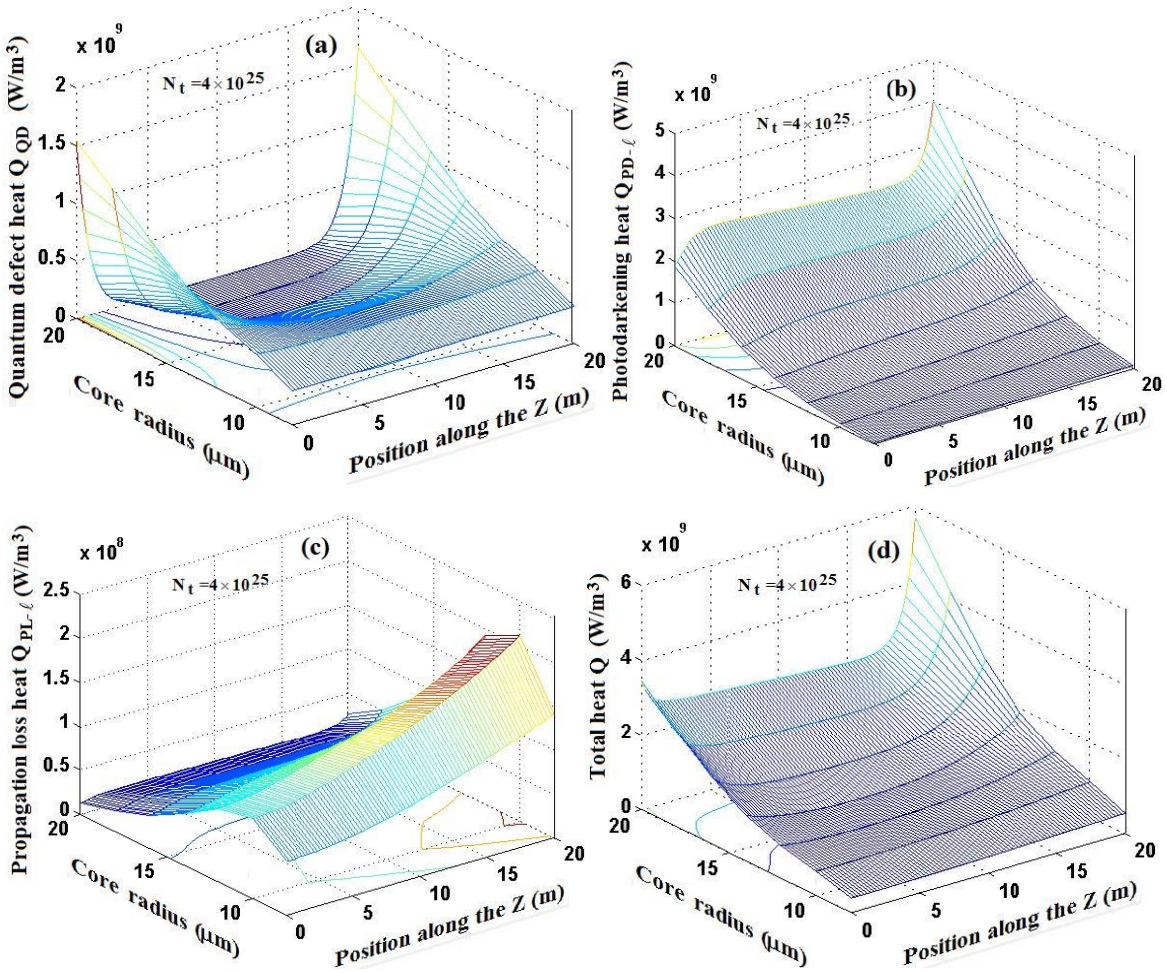

Fig. 4. 3D variation of a) Q_{QD} b) $Q_{PD-\ell}$ c) $Q_{PL-\ell}$ d) total heat, with respect to FL position a FL core radius.

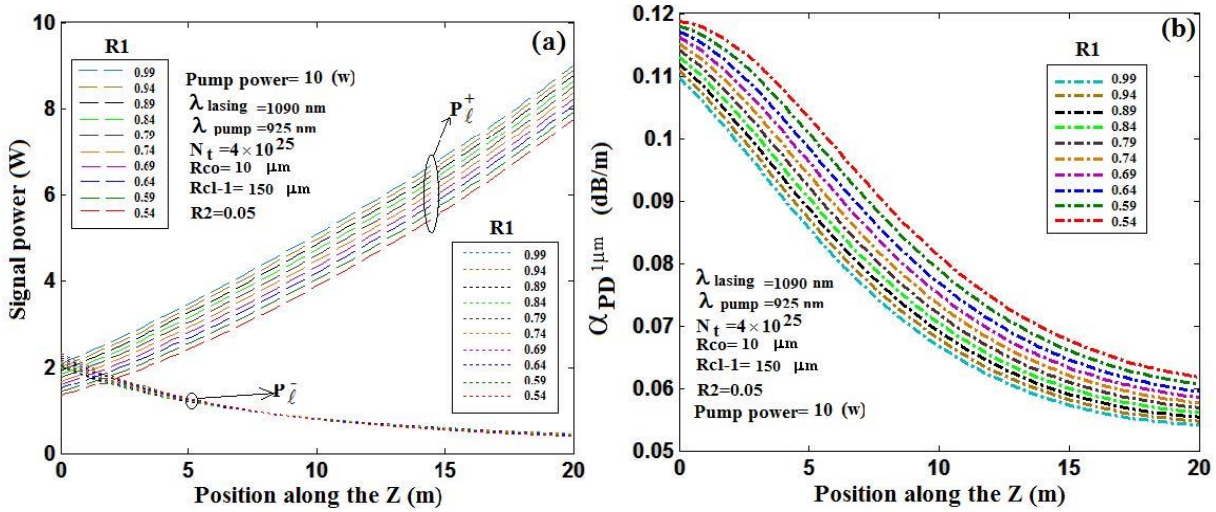

Fig. 5. a) FW and BW signal power variation along the FL position (b) variation of $\alpha_{PD^{1\mu m}}$ vs. the FL position for the different R1 values.

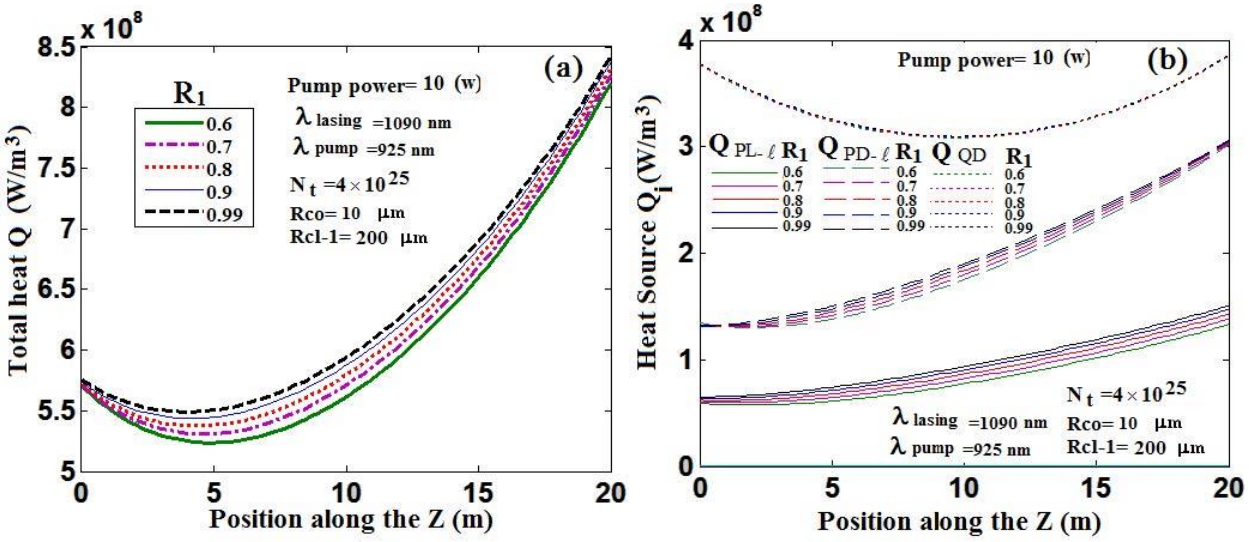

Fig. 6. (a) Total heat variation along the FL position (b) the share of QD, PD-ℓ, PL-ℓ in heat generation along the FL for different input refractive indices (R1).

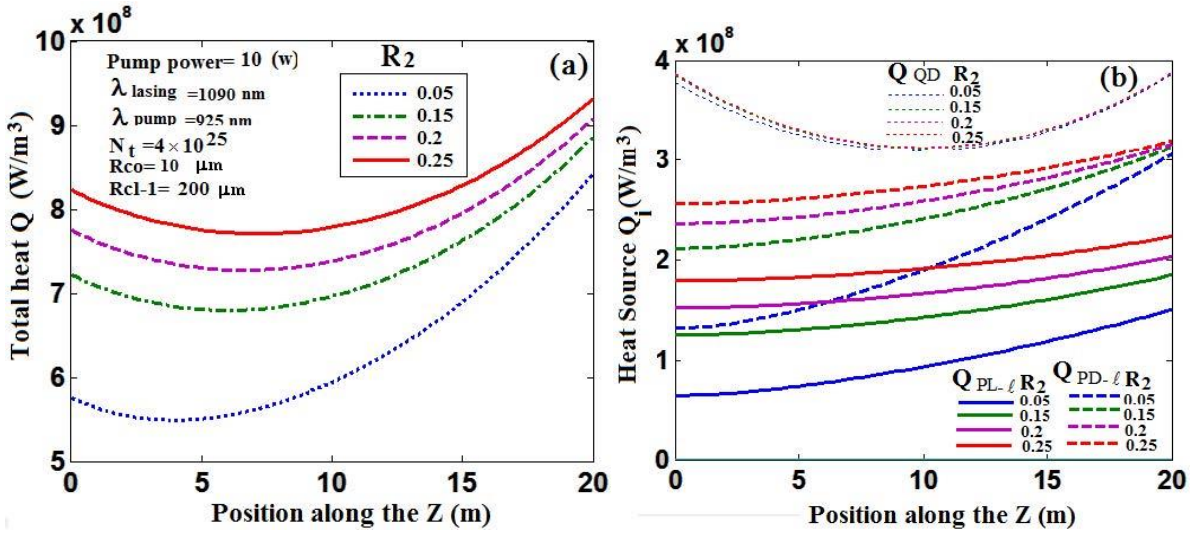

Fig. 7. (a) Total heat variation along the fiber position (b) the share of QD, PD-ℓ, PL-ℓ in heat generation along the FL for different output refractive indices (R2).

state resonator is investigated. It is shown that an increase in the reflection coefficient of the mirrors causes increase in the temperature of the resonator. Additionally, it has been demonstrated that getting away from the center of the mirror causes in decreasing the temperature in the longitudinal distance. In the present paper, the simulation shows a reduction in total heat, and therefore reduction in temperature in the longitudinal direction of Fiber Laser [47, 54-58].

From Fig. (6) to (9), the effects of the end put reflector on the heat distribution of FL are considered. In Figs. (6) and (7), the core and clad sizes are 10 and 200 mm, respectively. In Figs. (8) and (9), they are 10 and 150 mm, respectively. For different input reflector coefficient, the total heat variation with respect to fiber position is depicted in Fig. (6a). Using the higher reflection coefficient R1 in designing FL causes in increasing the heat generated in FL. In the FL with the higher reflection coefficient, the value of the signal power increases at the output end of FL in compression to the lower input reflection coefficient (see Fig. (5a)). For different input reflector coefficients, the contribution of each factor in Q_{QD}, $Q_{PD-\ell}$, and $Q_{PL-\ell}$ for the heat distribution was presented in Fig (6b). Increasing the first reflector coefficient does not have an effect on Q_{QD} agent because R1 is a reflector at signal (laser) wavelength. In Eq. (13), Q_{QD} associated only with pump power. By varying the R1 value, the pump power will be no change. However, in this condition, by increasing the signal

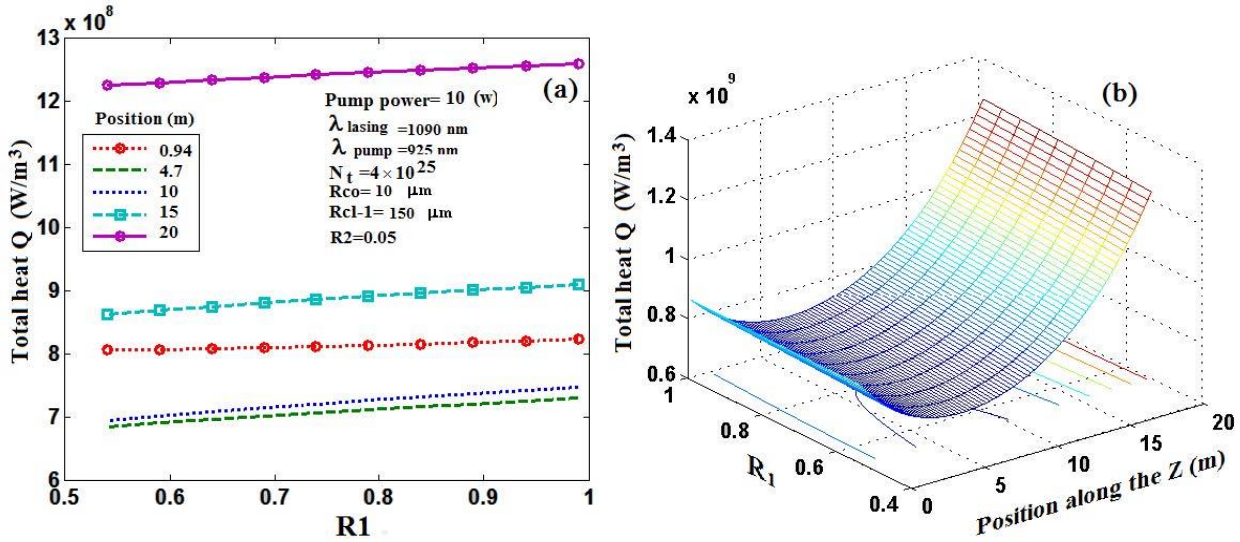

Fig. 8. ((a) Heat variation vs. input reflector coefficient-R1, (b) 3D variation of total generated heat with respect to FL position and R1.

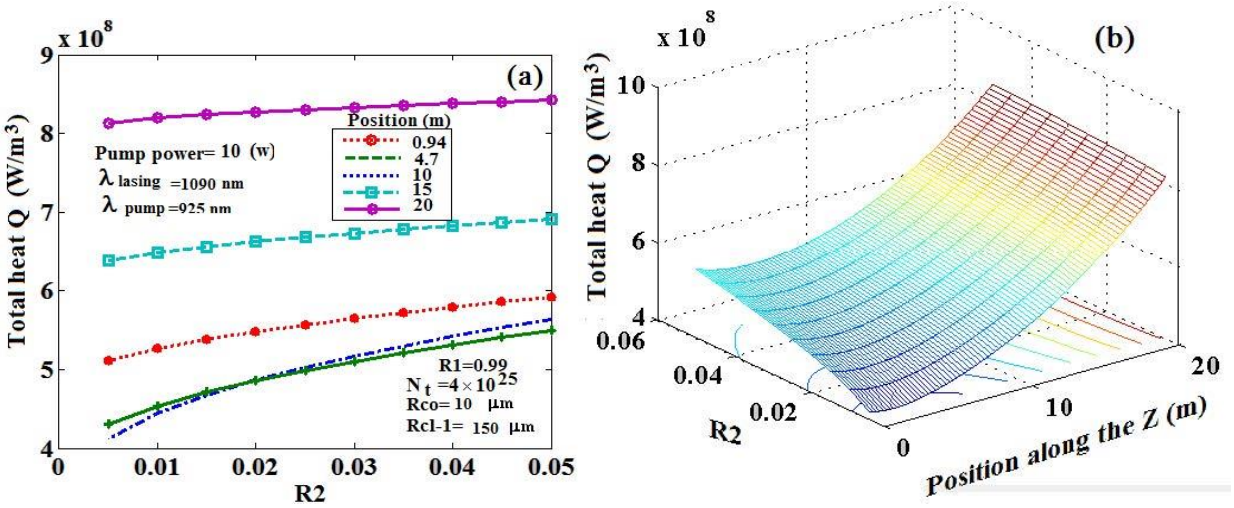

Fig. 9. (a) Heat variation vs. input reflector coefficient-R2, (b) 3D variation of total heat generation with respect to FL position and R2.

power, the value of the $Q_{PL-\ell}$, and $Q_{PD-\ell}$ have increased.

In Fig. (7a), the variation of the generated heat with respect to FL position for different value of R2 coefficient is depicted. As shown in this figure, the variation of R2 coefficient has a large effect on the generated heat in the input and middle points of FL. In comparison to Fig. (6a), the effect of the reflector coefficient is clearer on the opposite direction of FL. In Fig. (7b), the contribution of each factor in heat generation with respect to FL position for different R2 coefficient was depicted. In this case, the effect of the R2 coefficient at the Q_{QD} factor is negligible; but by increasing the R2 coefficient, it cause increases to the $Q_{PD-\ell}$, and $Q_{PL-\ell}$ with a large magnitude.

Fig. (8a) shows the variation of the generated heat with respect to R1 for different FL positions. As shown in Fig. (8a), the total generated heat has a weak dependency on the input reflector coefficient at any FL length, which can be ignored. In comparing the end point of FL (z=20 m) to the length of z=10 or 5 m, the generated heat is approximately twofold. Fig. (8b) shows the 3D dimension variation of the heat generation with respect to R1 and FL position.

Fig. (9a), shows the generated heat variation with respect to the R2 coefficient for different FL positions. In the comparison of Figs (8a) and (9a), the results show that the effect of the second mirror reflection coefficient on heat

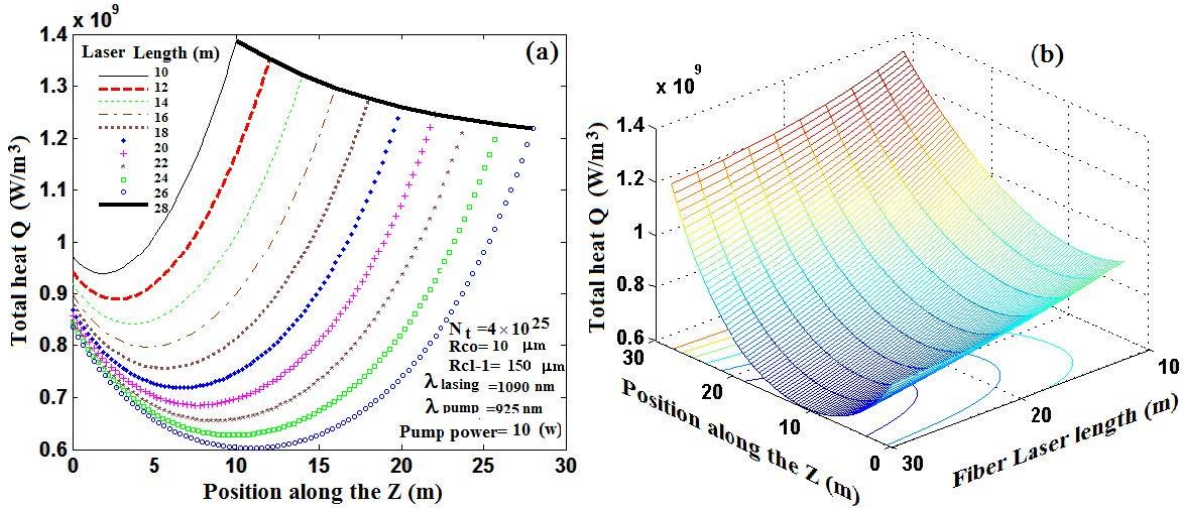

Fig. 10. a) Total heat variation with respect to the FL position in the FLs with the different length b) 3D variation of the total heat with respect to the laser length and the FL position.

generation in FL is greater. The increase of about 0.05 in the second mirror reflection, causes increment of about 0.5×10^8 W/m3 in the heat generation, while for an increase about 0.5 in the first mirror reflection, causes increment of about 0.5×10^8 W/m3 in the heat generation. Fig. (9b) shows a 3D variation of the heat generation with respect to R2 and the FL position.

In Fig. (10), the total generated heat in FLs with different cavity lengths is investigated. As shown in Fig. (10a), the heat (Temperature) variations are significant at any FL length. In the FLs with longer length than that of 25 m. This variation has a moderate form. The filled black curve shows the envelop temperature variation in FLs with different lengths, which shows that in the FL with the longer active area, the FL has the lower temperature at the end point. Therefore, it is expected that the MI is more observed in FLs with the shorter cavity length. The MI threshold must be lower on it. In FLs with the longer cavity length, the temperature decreases rapidly in the midpoint of FL. Fig. (10b), shows the 3D variation of the heat generation in FLs with different length and position in the FL. By solving the quartic functions of Eq. (17) and replacing the obtained results in Eq. (18), it causes determination of T 0. Using Eq. (19-21), the temperature can be determined at all FL regions.

The result of temperature variations with respect to the FL position, for different FL radius is depicted in Fig. (11a). As shown in this figure, the temperature has the minimum value at the central points of FL, and the temperature decreases by moving toward the FL surface. In Fig. (11b), the isothermal curves in FL in terms of the fiber radius and the FL position are shown. It should be noted that the optical nonlinear effect increases in the long length of FL, but the thermal effect and Mode Instability decreases in the long length of the FL. Thus, there must be a compromise between these two effects in designing of high-power FL.

5- Conclusion

This phenomenon occurs at a low pump level at the ordinary fibers (without dopant load). In practice, this phenomenon is usually not considered in the low-power Fiber Laser due to its small effect. In the present paper, PD induced loss in high power Yb doped fiber is considered.

The additional attenuation effect from PD phenomena has been considered in the rate equation. Although the author suggests the stretched exponential function for the PD effect with the variable of power, the author has used a constant value for the excess loss of PD effect because of the unavailability of the experimental values of the constants for suggested function to insert at this paper.

It was shown that the share of Q_{PD}^{P} , Q_{PL}^{P} in heat generation in the Double clad FL is negligible. In FLs with the small first clad size, the QD is the main factor in heat generation at the input and output points of FL. However, the PD-ℓ is the main factor in heat generation at the central points of FL.

The effect of cavity characters on heat distribution in FL was investigated using the complete form of the heat transfer function.

In FLs with the small core size, the PD-ℓ is the main factor in heat generation. In the FLs with the larger core size, the were more generated heat at the FL due to the presence of more dopant population in the core.

The effect of the input reflector at the P_{ℓ}^{+} , P_{ℓ}^{-} , and $\alpha_{PD-\ell}$ were investigated and shown that by increasing the reflector coefficient, the P_{ℓ}^{+} increased and P_{ℓ}^{-} decreased. The value of $\alpha_{PD-\ell}$ was calculated and showed that by increasing the input reflector coefficient, the value of $\alpha_{PD-\ell}$ increases.

The effect of the input reflector at heat generation is determined and showed that at the output points of the FL, the input reflector coefficient has the negligible effect of the heat or temperature variation. Additionally, the input reflector coefficient effect on each part of the heat generation element

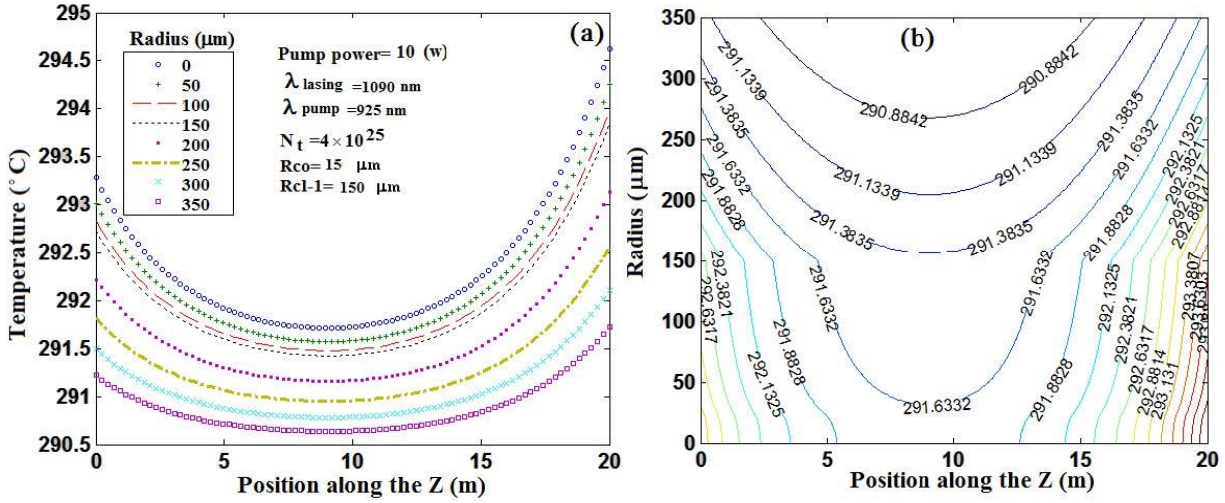

Fig. 11. a) Temperature variation with respect to the FL position at the different radius, b) Isothermal regions at the FL with the specific parameters.

is verified and shows that the first reflector has no effect on Q_{QD} . The effect of the output reflector in the heat generation is more significant than the input reflector, especially by increasing the second reflector coefficient the generated heat from the PD factor in the input points of FL increased rapidly. However, the generated heat from the QD agent is also negligible in this case.

In the FL with the short cavity length, the temperature was quickly increased and therefore the possibility of MI creation in the short FLs is higher than long FLs, and it is expected that the MI threshold be lower at the short FLs.

References

[1] H. W. Etzel, H. W. Candy, and R. J. Ginther, "Stimulated emission of infrared radiation from ytterbium activated silicate glass," Appl. Opt., Vol. 1, (1962) p. 534.

[2] H. M. Pask, Robert, J. Carman, D. C. Hanna, A. C. Tropper, C. J. Mackechnie, P. R. Barber, and J. M. Dawes, "Ytterbium-Doped Silica Fiber Laser s: Versatile Sources for the 1-1.2 pm Region", IEEE J. selected top. In quant. Electron., Vol. 1, (1995) 2-13.

[3] J. Oewiderski, A. Zajac, M. Skórczakowski, Z. Jankiewicz, and P. Konieczny, "Rare-earth-doped high-power Fiber Laser s generating in near infrared range", Opto-Electronics Review 12(2) (2004)169-173.

[4] A. V. Smith, and J. J. Smith, "Mode Instability thresholds for Tm-doped fiber amplifiers pumped at 790 nm", Opt. express. Vol. 24, (2016) 975-992.

[5] C. Jauregui, T. Eidam, H. J. Otto, F. Stutzki, F. Jansen, J. Limpert, and A. Tünnermann, "Temperature induced index gratings and their impact on mode instabilities in high-power fiber", laser systems", Opt. Express, Vol. 20, (2011) 440–451.

[6] C. Jauregui, J. Limpert, and A. Tünnermann, "Derivation of Raman treshold formulas for CW double-clad fiber amplifiers," Opt. Express 17 (2009) 8476–8490, 2009.

[7] S. Ramachandran, J. Fini, M. Mermelstein, J. W. Nicholson, S. Ghalmi, and M. F. Yan, "Ultra-large effective area, higher-order mode fibers: a new strategy for high-power lasers", Laser & Photon. Rev. 2, (2008) 429–448.

[8] N. G. R. Broderick, H. L. Offerhaus, D. J. Richardson, R. A. Sammut, J. Caplen, and L. Dong, "Large Mode Area Fibers for High Power Applications", Optical Fiber Technol., 5 (1999) 185-196.

[9] S. Saitoh, K. Saitoh, M. Kashiwagi, S. Matsuo,and L. Dong, "Design Optimization of Large-Mode-Area All-Solid Photonic Bandgap Fibers for High-Power Laser Applications", J. Lightwave Technol., 32, (2014) 440-449.

[10] K. Li, Y. Wang, W. Zhao, G. Chen, Q. Peng, D. Cui, and Z. Xu, "High power single-mode Large-Mode-Area photonic crystal Fiber Laser with improved Fabry-Perot cavity", Chinese Optics Letters, 4, (2006) 522-524.

[11] G. P. Agrawal, "Applications of Nonlinear Fiber Optics", Second edition, Academic Press, printed in the United States of America, Copyright c 2008.

[12] Z. Li, Z. Huang, X. Xiang, X. Liang, H. Lin, S. Xu, Z. Yang, J. Wang, and F. Jing, "Experimental demonstration of transverse Mode Instability enhancement by a counter-pumped scheme in a 2 kW all-fiberized laser", Photonics Research, 5, (2017) 77-81.

[13] K. H. Lee, K. Lee, Y. Kim, Y. H. Cha, G. Lim, H. Park, H. Cho, and D. Y. Jeong, "Transverse Mode Instability induced by Stimulated Brillouin Scattering in a pulsed single-frequency large-core fiber amplifier", App. Opt., 54 (2015) 189-194.

[14] I.O. Zolotovskii, D.A. Korobko, V.A. Lapin,

P.P. Mironov, D.I. Sementsov, A.A. Fotiadi, M.S. Yavtushenko, "Generation of subpicosecond pulses due to the development of modulation instability of whispering-gallery-mode wave packets in an optical waveguide with a travelling refractive-index wave", Quant. Electron. 48 (2018) 818 – 822.

[15] R. Tao, H. Xiao, H. Zhang, J. Leng, X. Wang, P. Zhou, and X. Xu, "Dynamic characteristics of Stimulated Raman Scattering in high power fiber amplifiers in the presence of mode instabilities", Opt. Express., 26 (2018) 25095-25110.

[16] J. P. Koplow, D. A. V. Kliner, L. Goldberg, "Single-mode operation of a coiled multimode fiber amplifier", Opt. Lett., Vol. 25,(2000), 442-444.

[17] M. Karimi, "Theoretical Study of the Thermal Distribution in Yb-Doped Double-Clad Fiber Laser by Considering Different Heat Sources", Progress in Electromagnetics Research C, 88, (2018) 59–76.

[18] C. Jauregui, H. J. Otto, F. Stutzki, J. Limpert, and A. Tünnermann1, "Simplified modelling the Mode Instability threshold of high-power fiber amplifiers in the presence of photodarkening", Opt. Express., 23, (2015) 20203- 20218.

[19] B. Ward, "Theory and modeling of photodarkening induced quasi static degradation in fiber amplifiers", Opt. Express., 24, (2016) 3488-3501.

[20] C. Ye, L. Petit, J. J. Koponen, I-N. Hu, and A. Galvanauskas, "Short-Term and Long-Term Stability in Ytterbium-Doped High-Power Fiber Laser s and Amplifiers", ieee. j. sel. top. quantum. electron., 20, (2014) 0903512.

[21] M. Engholm, M. Tuggle, C. Kucera, T. Hawkins, P. Dragic, and J. Ballato, "On the origin of photodarkening resistance in Yb-doped silica fibers with high aluminum concentration", Opt. Materials Express, 11, (2021) 115-125.

[22] H. Z. Li, L. Zhang, R. Sidharthan, Daryl Ho, X. Wu, N. Venkatram, H. D. Sun, T. Y. Huang, S. Yoo, "Pump Wavelength Dependence of Photodarkening in Yb-doped Fibers", J. Lightwave Technol., 35, (2017) 2535 – 2540.

[23] R. Cao, X. Lin, Y. Chen, Y. Cheng, Y. Wang, Y. Xing, H. Li, L. Yang, G. Chen, and J. Li, "532 nm pump induced photo-darkening inhibition and Photo-Bleaching in high power Yb-doped fiber amplifiers", Opt. Express, 27, (2019), 26523-26531.

[24] R. Cao, G. Chen, Y. Chen, Z. Zhang, X. Lin, B. Dai, L. Yang, AND J. Li, "Effective suppression of the photodarkening effect in high-power Yb-doped fiber amplifiers by H2 loading", Photonics Research, Vol. 8, pp. (2020), 288-295.

[25] R. Peretti, C. Gonnet, A. Marie Jurdyc, "A new vision of photodarkening in yb3+-doped fibers", Optical Components and Materials IX, Proc. of SPIE, 8257, (2012), 825705.

[26] R. Peretti, C. Gonnet, and A. Marie Jurdyc, "Revisiting literature observations on photodarkening in Yb3+doped fiber considering the possible presence of Tm impurities", App. Phys., 112, (2012), 093511.

[27] S. Liu, K. Peng, H. Zhan, L. Ni, X. Wang, Y. Wang, Y. Li, J. Yu, L. Jiang, R. Zhu, J. Wang, F. Jing, and A. Lin, "3 kW 20/400 Yb-doped alumino-phospho-silicate fiber with high stability," IEEE Photon. J. 10, (2018) P. 1503408.

[28] R. Sidharthan1, H. Li, K. J. Lim, S. H. Lim, Y. M. Seng1, S. L. Chua and S. Yoo, "Photo darkening suppression in highly Yb-doped Aluminophosphosilicate fiber by addition of Cerium", IEEE. Conference on Lasers and Electro-Optics Europe (CLEO EUROPE), 17, October (2019), 23-27.

[29] R. Cao, G. Chen, J. Li, "Eliminating photodarkening effect by H2-loading in high power Yb-doped fiber amplifiers", IEEE. Conference: CLEO: Science and Innovations, 2020.

[30] J. Jasapara, M. Andrejco, D. DiGiovanni, and R. Windeler, "Effect of heat and H2 gas on the photo-darkening of Yb+3 fibers", IEEE. Conference on Lasers and Electro-Optics. Quantum Electronics and Laser Science Conference, INSPEC Accession Number, (2006) P. 10363283.

[31] M. S. Kuznetsov, O. L. Antipov, A. A. Fotiadi, and P. Mégret, "Electronic and thermal refractive index changes in Ytterbium-doped fiber Amplifiers", Opt. Express., 21, (2013) 22374- 22388.

[32] S. Yoo, C. Basu, A. J. Boyland, C. Sones, J. Nilsson, J. K. Sahu, and D. Payne, "Photodarkening in Yb-doped

[33] aluminosilicate fibers induced by 488 nm irradiation", Opt. Let., 32 (2007) 16261628.

[34] J. Koponen, M. Söderlund, H. J. Hoffman, D. A. V. Kliner, J. P. Koplow, and M. Hotoleanu, Photodarkening rate in Yb-doped silica fibers", App. Opt. 47 (2008) 1247-1256.

[35] J. J. Koponen, M. J. Söderlund, S. K. T. Tammela, H. Po, "Photodarkening in ytterbium-doped silica fibers", proceedings of SPIE Security & Defense Europe '05 Symposium, Society of Photo-Optical Instrumentation Engineers.2005.

[36] F. Mady, M. Benabdesselam, Y. Mebrouk and B. Dussardier, "Radiation effects in ytterbium-doped silica optical fibers: traps and color centers related to the radiation-induced optical losses", RADECS 2010 Proceedings – Paper LN2,

[37] M. Engholm, P. Jelger, F. Laurell, and L. Norin, "Improved photodarkening resistivity in ytterbium-doped Fiber Laser s by cerium codoping", Opt. Lett., 34, (2009) 1285-1287.

[38] C. Jauregui, F. Stutzki, A. Tünnermann, and J. Limpert, "Thermal analysis of Yb-doped high-power fiber amplifiers with Al:P co-doped cores", Opt. Express., 16, (2018) 15540-15545.

[39] H. Gebavi, S. Taccheo, D. Tregoat, A. Monteville, and T. Robin, "Photobleaching of photodarkening in ytterbium doped aluminosilicate fibers with 633 nm irradiation", Opt. Mat. Express., 2, (2012) 1286-1291.

[40] L. Xiao, P. Yan, M. Gong, W. Wei, P. Ou, "An approximate analytic solution of strongly pumped Yb-doped double-clad Fiber Laser s without neglecting the scattering loss", Opt. commun. 230, (2004) 401-410.

[41] P. Leproux and S. F´evrier, "Modeling and Optimization

of Double-Clad Fiber Amplifiers Using Chaotic Propagation of the Pump", Optical Fiber Technol., 6, (2001) 324–339.

[42] D. Kouznetsov, and J. V. Moloney, "Highly Efficient, High-Gain, Short-Length, and Power-Scalable Incoherent Diode Slab-Pumped Fiber Amplifier/Laser", IEEE J. Quant. Electron., 39, (2003) 1452-1461.

[43] M. Leich, U. Röpke, S. Jetschke, S. Unger, V. Reichel, J. Kirchhof, "Non-isothermal bleaching of photodarkened Yb-doped fibers", Opt. Express., 17 (2009) 12588-12593.

[44] P. Yan, X. Wang, Y. Huang, C. Fu, J. Sun, Q. Xiao, D. Li, and M. Gong, "Fiber core mode leakage induced by refractive index variation in high-power Fiber Laser", Chin. Phys. B, 26, (2017) 034205.

[45] J. Li, K. Duan, Y. Wang, X. Cao, W. Zhao, Y. Guo, and X. Lin, "Theoretical analysis of the heat dissipation mechanism in Yb3+-doped double-clad Fiber Laser s", J. Modern Optic. 55, (2008) 459–471.

[46] J. Li, Y. Chen, M. Chen, H. Chen, X. Jin, Y. Yang, Z. Dai, Y. Liu, "Theoretical analysis and heat dissipation of mid-infrared chalcogenide fiber Raman laser", Opt. Commun., 284, (2011) 1278–1283.

[47] M. Sabaeian, H. Nadgaran, M. De Sario, L. Mescia, F. Prudenzano, "Thermal effects on double clad octagonal Yb:glass Fiber Laser", Optical Materials, 31, (2009) 1300–1305.

[48] P. Yan, Anan Xu, and Mali Gong, "Numerical analysis of temperature distributions in Yb-doped double-clad Fiber Laser s with consideration of radiative heat transfer", Opt. Engin. 45, (2006) 124201.

[49] S. Neumark, "Solution of Cubic and Quartic Equations", Pergam on Press, Oxford London, First edition, 1965.

[50] D. Polyanin, A. V. Mainchirov, Handbook of mathematics for engineers and scientist, Chapman &Hall/CRC Press, Taylor & Francis Group, Danvers, 2007.

[51] Z. Luo, C. Ye, G. Sun, Z. Cai, M. Si, Q. Li, "Simplified analytic solutions and a novel fast algorithm for Yb3+-doped double-clad Fiber Laser s", Opt. Commun., 277, (2007) 118–124.

[52] F. Brunet, Y. Taillon, P. Galarneau, and S. LaRochelle, "Practical Design of Double-Clad Ytterbium-Doped Fiber Amplifiers Using Giles Parameters", IEEE J. Quant. Electron., 40, (2004) 1294-1300.

[53] I. Kelson and A. Hardy, "Optimization of Strongly Pumped Fiber Laser s«, J. of Ligthwave Technol. 17 (1999) 891-897.

[54] S. Taccheo, H. Gebavi, A. Monteville, O. Le Goffic, D. Landais, D. Mechin, D. Tregoat, B. Cadier, T. Robin, D. Milanese, and T. Durrant, "Concentration dependence and self-similarity of photodarkening losses induced in Yb-doped fibers by comparable excitation", Optics Express, 19, (2011), 19340-19345.

[55] Y. Peng, Z. Cheng, Y. Zhang, and J. Qiu, "Temperature distributions and thermal deformations of mirror substrates in laser resonators", App. Opt. Vol. 40, (2001) 4824-4830.

[56] Y. Lv, S. Liu, "Heat dissipation model and temperature distribution of Yb-doped double clad fiber in the composite system", Opt. Fiber Technol., Vol. 58, (2020) 102269.

[57] Esmaeil Mobini, Mostafa Peysokhan, Behnam Abaie, and Arash Mafi, "hermal modeling, heat mitigation, and radiative cooling for double-clad fiber amplifiers", Journal of the Optical Society of America B, Vol. 35, (2018) 2484-2493

[58] P. Li, C. Zhu, Meng Chen, S. Zou, H. Zhao, D. Jiang, G. Li, M. Chen, "Theoretical and experimental investigation of thermal effects in a high power Yb3+-doped double-clad Fiber Laser", Optics and Laser Technology, (2007) 119477463.

[59] Y. Wang, C. Q. Xu; H. Po, "Thermal effects in kilowatt Fiber Laser s", IEEE. Photon. Technol. Lett., Vol. 16, pp. 63 – 65, 2004.

HOW TO CITE THIS ARTICLE

M. Karimi, Heat Distribution in High Power Yb Doped Fiber Laser by Considering Photo-darkening Effect, AUT J. Model. Simul., 53(2) (2021) 137-152.

DOI: 10.22060/miscj.2022.19713.5242